1 2 3	Classification PHYSICAL SCIENCES: Biophysics PHYSICAL SCIENCES: Engineering Science
5	<b>Title:</b> Mechanical stress compromises multicomponent efflux complexes in bacteria
7 8 9 10	Lauren A. Genova <sup>a,1</sup> , Melanie F. Roberts <sup>b,1</sup> , Yu-Chern Wong <sup>b</sup> , Christine E. Harper <sup>c</sup> , Ace George Santiago <sup>a,d</sup> , Bing Fu <sup>a</sup> , Abhishek Srivastava <sup>b,e</sup> , Won Jung <sup>a</sup> , Lucy M. Wang <sup>b,f</sup> , Łukasz Krzemiński <sup>a,g</sup> , Xianwen Mao <sup>a</sup> , Xuanhao Sun <sup>b,h</sup> , Chung-Yuen Hui <sup>b</sup> , Peng Chen <sup>a,2</sup> , Christopher J. Hernandez <sup>b,c,2</sup>
11 12 13 14 15 16 17 18 19 20 21 22	<sup>a</sup> Department of Chemistry and Chemical Biology, Cornell University, Ithaca, NY, USA. <sup>b</sup> Sibley School of Mechanical and Aerospace Engineering, Cornell University, Ithaca, NY, USA. <sup>c</sup> Meinig School of Biomedical Engineering, Cornell University, Ithaca, NY, USA. <sup>d</sup> Present address: Department of Microbiology and Immunobiology, Harvard Medical School, Boston, MA, USA. <sup>e</sup> Present address: Corporate Research Laboratory, 3M Company, St. Paul, MN, USA. <sup>f</sup> Present address: Department of Mechanical Engineering, Stanford University, Stanford, CA, USA. <sup>g</sup> Present address: OncoArendi Therapeutics SA, Żwirki i Wigury 101, 02-089 Warsaw, Poland. <sup>h</sup> Present address: Department of Physiology and Neurobiology, University of Connecticut, Storrs, CT, USA.
<ul><li>23</li><li>24</li></ul>	<sup>1</sup> L.A.G. and M.F.R. contributed equally to this work. <sup>2</sup> To whom correspondence should be addressed. Email:
25 26	(C.J.H.) <u>cjh275@cornell.edu</u> , Sibley School of Mechanical & Aerospace Engineering, Cornell University, 355 Upson Hall, Ithaca, NY 14853. ORCID: <u>0000-0002-0712-6533</u>
27 28 29 30	(P.C.) <u>pc252@cornell.edu</u> , Department of Chemistry & Chemical Biology, Cornell University, Ithaca, NY 14853. <u>ORCID: 0000-0001-8582-7661</u>
31	<b>Author contributions</b>
32 33 34 35 36 37 38 39 40 41	L.A.G. prepared cell strains, performed single-molecule imaging, analyzed the mechanical effects on efflux complex assembly, and curated data. M.F.R. fabricated microfluidic devices, performed mechanical manipulation, analyzed cell mechanical stresses, and curated data. YC.W. performed mechanical modeling. L.A.G. and M.F.R. performed cell growth assays. A.G.S., B.F., W.J., X.M., C.E.H., L.M.W., and Ł.K. contributed to experiments and data analysis. X.S. contributed to microfluidic device design. A.S. contributed to mechanical modeling. CY.H. supervised mechanical modeling. L.A.G., M.F.R., YC.W., C.E.H., P.C., and C.J.H. analyzed/discussed results and wrote the manuscript. P.C. and C.J.H. conceived and directed research.

42 43	The authors declare no conflict of interest.
44	This article is a PNAS Direct Submission.
45	
46	Keywords
47	
48	Extrusion loading, single-molecule imaging, multicomponent efflux complex, diffusion
49	dynamics, octahedral shear vs. hydrostatic stress

#### **Abstract**

50 51 52

53

54

55

5657

58

59

60

61

62 63

64

65

66

67

68

69

Physical forces have a profound effect on growth, morphology, locomotion, and survival of organisms. At the level of individual cells, the role of mechanical forces is well recognized in eukaryotic physiology, but much less is known about prokaryotic organisms. Recent findings suggest an effect of physical forces on bacterial shape, cell division, motility, virulence, and biofilm initiation, but it remains unclear how mechanical forces applied to a bacterium are translated at the molecular level. In Gram-negative bacteria, multicomponent protein complexes can form rigid links across the cell envelope and are therefore subject to physical forces experienced by the cell. Here we manipulate tensile and shear mechanical stress in the bacterial cell envelope and use single-molecule tracking to show that octahedral shear (but not hydrostatic) stress within the cell envelope promotes disassembly of the tripartite efflux complex CusCBA, a system used by E. coli to resist copper and silver toxicity. By promoting disassembly of this protein complex, mechanical forces within the cell envelope make the bacteria more susceptible to metal toxicity. These findings demonstrate that mechanical forces can inhibit the function of cell envelope protein assemblies in bacteria and suggests the possibility that other multicomponent, trans-envelope efflux complexes may be sensitive to mechanical forces including complexes involved in antibiotic resistance, cell division, and translocation of outer membrane components. By modulating the function of proteins within the cell envelope, mechanical stress has the potential to regulate multiple processes required for bacterial survival and growth.

70 71 72

## **Significance Statement**

73 74 75

76

77

78

79

The field of mechanobiology examines how physical forces modulate cell physiology and has traditionally focused on eukaryotic organisms. Here we show that in bacteria, mechanical stresses can interrupt the structure and function of a molecular assembly used by Gram-negative bacteria to survive and grow in the presence of toxins. This work provides the first evidence that bacteria, like mammalian cells, can respond to mechanical forces through molecular complexes at the cell surface in ways that are relevant to growth. Our observations further suggest that mechanical forces may be used synergistically with other antimicrobials.

80 81 \body

Over 100 years ago the mathematical biologist D'Arcy Thompson in his book *On Growth and Form* argued for the role of physical forces in the development and morphology of organisms using examples including the shapes of wings, bones, shells and individual cells (1). Physical forces are now recognized as major contributors to embryogenesis (2), tissue healing (3), and the development of disease (4). While the effect of physical forces on cell physiology is well-recognized in eukaryotic systems, physical forces are also believed to be relevant to prokaryotes (5), although much less is known about their role in prokaryotic organisms including bacteria. Bacteria are ubiquitous in the environment and their sensitivity to physical forces has the potential to influence biotechnology, human health, diagnostics and biofouling.

Bacteria experience a wide range of mechanical stimuli in their environment including changes in osmolarity and hydrostatic pressure; as well as forces associated with adhesion to surfaces, locomotion, division, turbulent flows, and growth within constrained spaces (6-9). Rapid changes in osmolarity or hydrostatic pressure can influence cell growth and a variety of stretch activated channels (9), primarily by modulating surface tension in the cell envelope. The mechanical stresses experienced by the bacterial cell envelope during locomotion (10), surface adhesion (8, 11), and cell division (12) are more complicated than those associated with osmolarity and can include combinations of tensile (lengthening), compressive (shortening), and shear (shape changing) mechanical stresses. How a bacterium responds to these more complicated states of mechanical stress is not well understood.

In eukaryotic systems, the initial transmission of external forces to the cell often occurs through cell surface protein assemblies that cross the cell membrane (13). Bacteria contain many trans-envelope protein complexes. In Gram-negative bacteria, trans-envelope protein assemblies such as tripartite efflux complexes enable the bacteria to extrude a diverse set of antibiotics and other toxic chemicals, enabling bacterial multidrug resistance (14). CusCBA is a tripartite Cu<sup>+</sup> and Ag<sup>+</sup> efflux complex in *E. coli* and belongs to the resistance-nodulation-division (RND) family complexes that provide clinically relevant multidrug resistance to Gram-negative bacteria (14). CusA is a trimeric proton-motive-force–driven pump located in the inner-membrane; CusB is a periplasmic adaptor protein; CusC is a trimeric outer-membrane pore protein; these three proteins assemble into the complete CusC<sub>3</sub>B<sub>6</sub>A<sub>3</sub> complex to enable efflux of Cu<sup>+</sup>/Ag<sup>+</sup> from the cell (15-17). By tagging CusA with a photoconvertible fluorescent protein and using single-molecule tracking measurements, we previously found that inside cells, CusCBA exists in a dynamic equilibrium between an assembled and disassembled state; and this equilibrium is responsive to environmental increase of copper concentration and shifts toward the assembled state for effective efflux in defending against metal (e.g., copper) stress (18).

Here we use a microfluidic system to generate combinations of tension, compression and shear within the bacterial cell envelope to study the effects of mechanical stress on the function of protein complexes that span the envelope of Gram-negative cells. We demonstrate that cell envelope mechanical stress promotes disassembly of the CusCBA complex in *E. coli* cells and thereby enhances copper—induced reductions in cell reproduction and growth. We further show that the reduced assembly of CusCBA is not associated with tensile/compressive stresses (the

primary form of stress generated by osmolarity and hydrostatic pressure) but is correlated with octahedral shear stresses within the cell envelope.

128129130

127

# **Results and Analysis**

131 132

# Extrusion loading provides controlled mechanical stress on individual bacteria

133 134

135

136137

138 139

140

141

142

143

144

145146

147

148

149

150

151

To query the contributions of mechanical stress to bacterial physiology, we used a microfluidic device with submicron features to apply mechanical loads to individual bacteria. The device is analogous to micropipette aspiration commonly used to study mammalian cell biomechanics (19, 20) but instead of pulling the cell into a tapered channel, the device forces cells into tapered channels using fluid pressure (21). Each device contains sets of tapered channels to apply twelve distinct magnitudes of pressure difference ( $\Delta P$ ) across the trapped bacteria within a single experiment (Figs. 1A–B, and SI Appendix, Fig. S1). The pressure difference is controlled by modifying fluid pressure at the inlet (also affecting the average pressure,  $P_{\text{ave}}$ , which is indicative of hydrostatic pressure experienced by the cell) and determined locally with hydraulic circuit models (SI Appendix, section 1.2). We refer to this loading modality as "extrusion loading." Bacteria submitted to stepwise increases in  $\Delta P$ exhibited increases in cell length and decreases in cell width, resulting in a net reduction in cell volume (Fig. 1C and SI Appendix, Fig. S4). Analytical and finite element models indicate that extrusion loading causes increases in axial tensile stress and reductions in hoop (transverse) tensile stress, related to the magnitude of  $\Delta P$  (Fig. 1D and SI Appendix, Figs. S5 and S6). Furthermore, analytical examination shows that reductions in cell volume during extrusion loading result in an increase in cell internal pressure, which we attribute to increases in osmolarity associated with loss of water from the cytoplasm when cell volume declines.

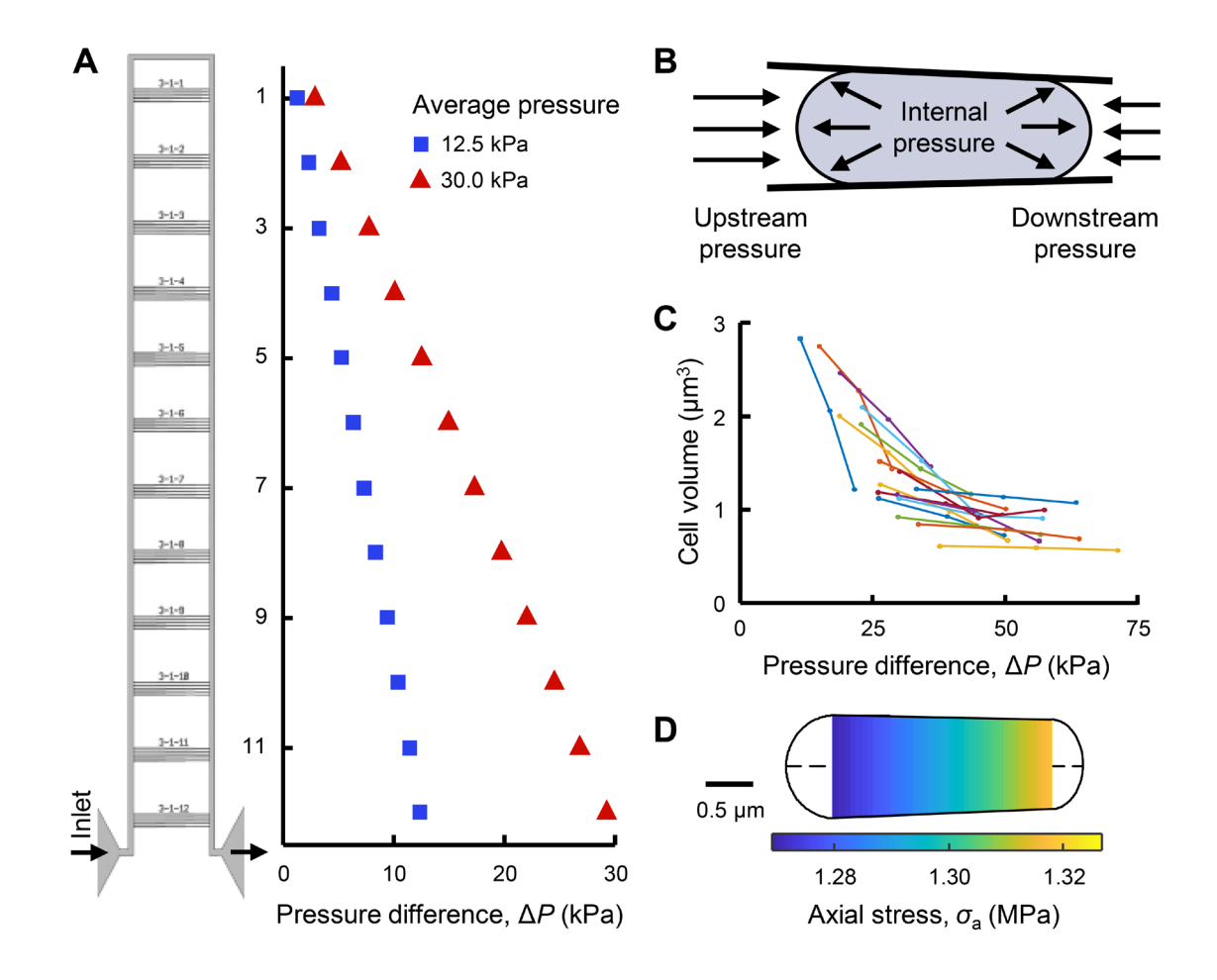


Fig. 1. Mechanical loading of bacteria via a microfluidic device. (A) A functional unit of the microfluidic device has twelve sets of five tapered channels. Fluid flow enters the functional unit at the bottom left, travels around the bypass channel, and exits out the bottom right. The difference between upstream and downstream pressure is larger for tapered channels closer to the inlet and outlet. Increasing the applied pressure increases the pressure difference  $\Delta P$  at each set of tapered channels (and also increases the average pressure,  $P_{\text{ave}}$ ). (B) Trapped bacteria experience greater upstream pressure than downstream pressure. The pressure difference  $\Delta P$  is defined as the difference between the upstream and downstream pressures. Internal pressure due to turgor is also present. (C) Increases in  $\Delta P$  via stepwise increases of externally applied pressure results in reduced cell volume of trapped cells. Lines connect measurements of same cells. (D) Analytical modeling of a trapped cell indicates a linear increase in axial stress along the length of the cell.

## Mechanical stress from pressure differentials disrupts the assembly of CusCBA in the cell

To understand the effects of mechanical stress on a trans-envelope complex, we examined the assembly of CusCBA in *E. coli* cells under extrusion loading (Fig. 1*B*). When assembled, CusCBA forms a rigid link across the cell envelope and is therefore subject to mechanical stress and strain experienced by the cell envelope. To probe the assembly of CusCBA, we tagged the C-terminus of the inner-membrane protein CusA by a photoconvertible fluorescent protein mEos3.2 (i.e., CusA<sup>mE</sup>) at its chromosomal locus (*SI Appendix*, section 1.7); this tagging ensures physiological expression of CusA<sup>mE</sup> in the cell. This fluorescent protein tag

also enables the use of sparse photoconversion and subsequent time-lapse stroboscopic fluorescence imaging to track the motions of individual photoconverted CusA<sup>mE</sup> proteins at tens of nanometer precision and 60 ms time resolution (Fig. 2*B*, inset) and quantify CusA<sup>mE</sup> copy number in each cell (18).

We examined hundreds of cells submitted to extrusion loading containing, in total, thousands of CusA<sup>mE</sup> proteins. These cells were in different tapered channels and sampled a large range of  $\Delta P$  (Fig. 2A), allowing us to sort the cells into groups of similar  $\Delta P$  and determine the relationship between the magnitude of extrusion loading and diffusive behaviors of tracked CusA<sup>mE</sup> proteins. Within assembled CusCBA complexes, the motion of CusA<sup>mE</sup> is severely restricted to be almost stationary, but CusA<sup>mE</sup> that is disassembled from the complex is highly mobile. These two diffusive states of CusA<sup>mE</sup> can be differentiated by analyzing the distribution of CusA<sup>mE</sup>'s single-molecule displacement lengths between adjacent image frames (Fig. 2B and SI Appendix, section 1.12) (18). After using an inverse transformation approach to deconvolute the effects of cell confinement and 2-D projection of 3-D motions (18, 22, 23), we could resolve the displacement length distribution into the two diffusive states across all applied pressure conditions: the stationary assembled state and the mobile disassembled state, along with diffusion constants and fractional populations (Fig. 2B and SI Appendix Fig. S11C). The resolution and assignment of these two diffusion states were validated previously by control measurements on the free mEos3.2 tag, single deletion strains missing CusC or CusB, and diffusion simulations (18).

Strikingly, the fractional population of the mobile disassembled state of CusA<sup>mE</sup> in the cell increases by a factor of ~2 when  $\Delta P$  increases from ~4 to ~25 kPa (Fig. 2C), indicating a direct association between the magnitude of extrusion loading and the disruption of CusCBA assembly in the cell. Concurrently, the effective diffusion constant of the mobile disassembled CusA<sup>mE</sup> decreases by a factor of ~4 across this range of  $\Delta P$ , while that of the stationary assembled CusCBA complex, which traverses the cell envelope, remains the same, as expected for stationary objects (Fig. 2D). We further conducted experiments where the applied pressure is zero and  $\Delta P$  is thus also zero on the trapped cells. The determined fractional population and diffusion constant of the mobile disassembled CusA<sup>mE</sup> remain on the same trends vs.  $\Delta P$  (Fig. 2C-D). These trends show that external mechanical stress can influence the assembly of the CusCBA complex as well as the diffusivity of mobile unassembled inner membrane proteins, the latter of which could have contributions from membrane fluidity changes from mechanical stress (24).

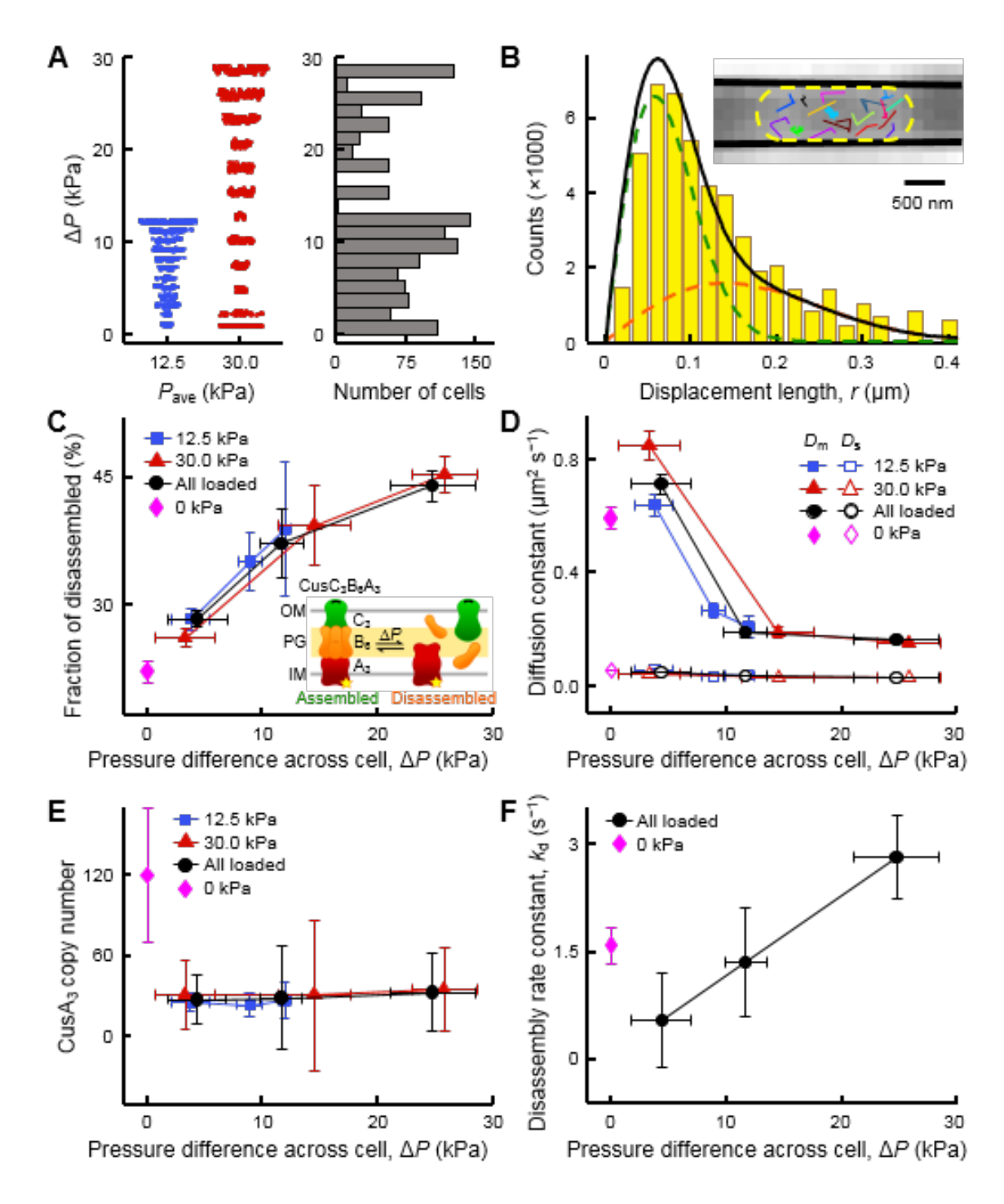


**Fig. 2.** Single-molecule tracking uncovers mechanical stress-induced CusCBA disassembly. (*A*) Cells were examined at two applied external loading conditions resulting in average pressure values of 12.5 kPa (n = 592 cells; blue points) and 30.0 kPa (n = 732 cells; red points), giving a range of Δ*P* across individual cells. (*B*) Distribution of displacement length r per time lapse for single CusA<sup>mE</sup> proteins at  $P_{ave} = 30.0$  kPa and  $\Delta P = 24.7 \pm 3.7$  kPa, in which the cell confinement effect is deconvoluted (*SI Appendix*, section 1.12). The distribution here resolves minimally two Brownian diffusion states (Eq. S23): a mobile disassembled state (orange dashed line) and an almost stationary assembled state (green dashed line), with diffusion constants of  $D_m = 0.16 \pm 0.01$  μm<sup>2</sup> s<sup>-1</sup> and  $D_s = 0.027 \pm 0.001$  μm<sup>2</sup> s<sup>-1</sup> and fractional populations of  $A_m = 44 \pm 2\%$  and  $A_s = 56 \pm 2\%$ , respectively. Solid black line: overall fit. Inset: Overlay of many position trajectories of

single CusA<sup>mE</sup> proteins in a living *E. coli* cell trapped in a tapered channel. Each colored line is from one CusA<sup>mE</sup>. Yellow dashed line: cell boundary; solid black lines: inner walls of the tapered channel. (*C*) Fractional populations of the mobile disassembled state of CusA<sup>mE</sup> increases with increasing  $\Delta P$  at  $P_{ave} = 30.0$  kPa (red) or 12.5 kPa (blue). Black: results combining  $P_{ave} = 30.0$  and 12.5 kPa conditions. Magenta: results where  $P_{ave} = 0$  and  $\Delta P = 0$ . Color coding of points applies to *D-F* as well. Inset: CusCBA can dynamically shift between two forms: assembled (stationary, left) and disassembled (mobile, right). OM, outer membrane; PG, peptidoglycan; IM, inner membrane. Yellow star: mEos3.2-tag on CusA. (*D*) The diffusion constants of the mobile disassembled state ( $D_m$ ) and the stationary assembled state ( $D_s$ ) vs.  $\Delta P$  at different pressure conditions. (*E*) Copy number of CusA trimers (CusA<sub>3</sub>) vs.  $\Delta P$  at different pressure conditions. Error bars are s.d., and lines connecting the points are eye guides in C-F. Numerical values reported here are in mean  $\pm$  s.d.

Bacteria submitted to extrusion loading experience a pressure difference across the tapered channels ( $\Delta P$ ), as well as a hydrostatic pressure ( $P_{\rm ave}$ , the average between upstream and downstream pressures on a cell), both related to the fluid pressure applied at the device inlet. While the behaviors of CusA<sup>mE</sup> in response to  $\Delta P$  were substantial, the behaviors of CusA<sup>mE</sup> showed no significant differences when  $P_{\rm ave}$  changed by a factor of 2 (Fig. 2C–D, blue vs. red points); combining results from the two  $P_{\rm ave}$  conditions gave the same behaviors (Fig. 2C–D, black points). Therefore, hydrostatic pressure, at least within our experimental regime, does not play significant roles in membrane protein assembly and diffusivity, suggesting that mechanically-induced disassembly of CusCBA would not be observed using osmotic shock or hydrostatic pressure, two commonly used mechanical stimuli that primarily modify surface tension (25).

We further examined the copy number and spatial distribution of  $CusA^{mE}$  in all cells across the different pressure conditions. Neither of these two properties show noticeable changes with varying  $\Delta P$  or  $P_{ave}$  under applied pressure conditions (Fig. 2E and SI Appendix, Fig. S14), supporting the idea that modifications in CusCBA assembly induced by extrusion loading are likely not due to cell physiological changes such as CusA protein expression or intracellular localization.

We further analyzed the single-molecule displacement vs. time trajectories of CusA<sup>mE</sup> to estimate the underlying kinetics of CusA<sup>mE</sup> disassembly from the CusCBA complex. In these trajectories, transitions from small displacements to large ones predominantly reflect disassembly events (*SI Appendix*, Fig. S12 and section 1.13). The extracted effective disassembly rate constant increases from ~0.5 to ~2.8 s<sup>-1</sup> with increasing  $\Delta P$  (Fig. 2F), supporting the idea that mechanical stress compromises the stability of the assembled CusCBA complex in part by enhancing the disassembly rate. In the absence of applied pressure where  $\Delta P$  is also zero for all cells in the tapered channels, the effective disassembly rate constant as well as the copy number of CusA<sup>mE</sup> are slightly higher than those under applied pressures, but the differences are within or close to experimental errors (Fig. 2E and F).

## Mechanical stress enhances cell sensitivity to copper stress

Copper and silver are toxic to *E. coli*, impeding cell growth at low to moderate concentrations and causing cell death at high concentrations. CusCBA plays a crucial role in *E. coli*'s ability to resist the presence of copper (and silver) ions in the environment (17). The

mechanical stress—induced disassembly of CusCBA in the cell should therefore lead to a further reduction in cell growth under copper stress conditions. To confirm such functional effects, we examined how mechanical stress in extrusion loading affected elongation and reproduction of hundreds of individual *E. coli* cells by tracking cell length and time to division under copper stress. Rate of elongation and time to division were both examined in media with 0 or 2.5 mM CusO<sub>4</sub> (*SI Appendix*, Figs. S16 and S17). The maximum rate of elongation decreased with larger magnitudes of extrusion loading (greater  $\Delta P$ , Fig. 3*A*) and followed an exponential decay, consistent with known adverse effect of mechanical stress on bacterial growth (26-28). In the presence of copper stress, the exponential decay rate (0.38 ± 0.14 kPa<sup>-1</sup>, value ± SE) was substantially greater than that without copper stress (0.08 ± 0.04 kPa<sup>-1</sup>), indicating synergy between mechanical and copper stress in suppressing cell elongation (or division) (Fig. 3*A*). It is worth noting that the indiscernible difference with or without copper at  $\Delta P$  greater than ~20 kPa is due to a saturation effect – the growth has slowed by mechanical stress to an extent that additional copper stress would make little difference.

To confirm that the effects of mechanical stress on the function of CusCBA were not limited to extrusion loading in microfluidic chambers, we also assessed the effects of copper stress using an alternative mechanical loading approach: the growth of cells encapsulated in agarose gel with increasing stiffness (28, 29). We used three different concentrations of agarose (0, 0.25, and 0.5 w/v %), corresponding to three different levels of gel stiffness (SI Appendix, Fig. S13 and section 1.14) (it is worth noting that at agarose concentrations smaller than 0.25%, the solution does not form gels). The maximum growth rate of the E. coli population decreased in higher agarose concentration gels, consistent with a previous report (29) (Fig. 3B, black points). Expectedly, the presence of copper also decreases the cell growth rate (e.g., pink vs. black points in Fig. 3B). More important, in gels that impose mechanical resistance on cell growth, the copper-induced decrease in growth rate is greater in magnitude than that in the absence of gels (e.g., pink and black points at 0.25% vs. at 0.0% agarose in Fig. 3B), indicating that mechanical stress enhances the toxic effects of copper ions on growth. It is worth noting that such agarose gel encapsulation does not restrict nutrient access to the cells (28, 29). Taken together, the results from extrusion loading and agarose gel embedding support that mechanical stress-induced disassembly of CusCBA enhances the toxic effects of copper stress on bacterial physiology.

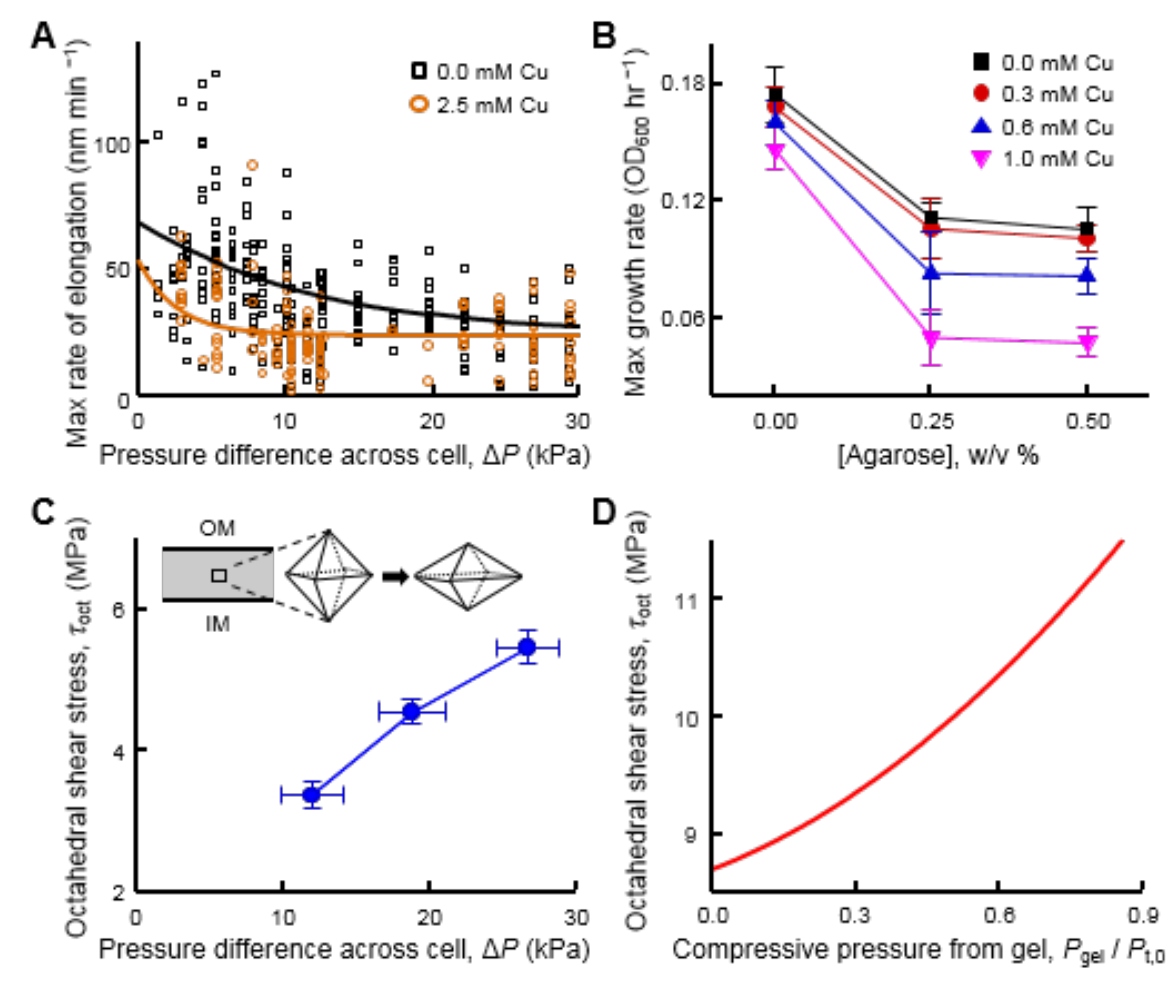


Fig. 3. Mechanical loading enhances the toxic effects of copper stress on elongation and growth of  $E.\ coli.$  (A) Maximum growth rate (elongation) of individual cells under extrusion loading without copper stress (n=253 cells) and with copper stress (n=134 cells). Solid lines display exponential decay fits. (B) Maximum growth rate of cells encapsulated in agarose gel without and with increasing copper stress. Maximum growth rate is influenced by copper concentration, agarose stiffness (concentration), and copper\*agarose (p=0.046 for all copper concentrations at 0% and 0.25% agarose conditions), indicating synergy between copper concentration and agarose stiffness ( $SI\ Appendix$ , section 1.14). Error bars are s.d. (C) Finite element analysis demonstrates that octahedral shear stress in the cell envelope of bacteria under extrusion loading increased with increasing  $\Delta P$ . Material properties used in the analysis are in  $SI\ Appendix$ , Table S3. Error bars are s.d. Inset: 3D depictions of the effects of octahedral shear stress (left) on an infinitesimal element located in the cell envelope. The volume does not change but the shape is distorted (compared with hydrostatic stresses, Fig. S7A inset). (D) Octahedral shear stress in the cell envelope of bacteria encapsulated in gel (growth confinement loading) increased with increasing compressive pressure from the gel ( $P_{gel}$ ). The compressive pressure was normalized to the assumed turgor pressure ( $P_{t,0}$ ), where a value of  $P_{gel}$  /  $P_{t,0}$  greater than 1.0 would result in buckling or collapse of the cell.

### Role of shear stress within the cell envelope

Extrusion loading and gel encapsulation techniques generate substantially different combinations of tensile, compressive, and shear stresses in the bacterial cell envelope (SI Appendix, section 1.6). To better understand the components of cell envelope stress associated with mechanically-enhanced disassembly of CusCBA and resulting enhancement of copper

sensitivity, we generated analytical and finite element models of the two mechanical loading modalities (*SI Appendix*, sections 1.5 and 1.6). Extrusion loading increases axial tension and reduces tensile hoop stresses while gel encapsulation reduces axial tension in the cell envelope with little effect on hoop stresses (*SI Appendix*, Fig. S6C).

To identify the forms of mechanical stress that promote disassembly of CusCBA, we decomposed the three-dimensional stress state within the cell envelope into a hydrostatic (volume-changing) component and an octahedral shear (shape-changing) component (Fig. 3C, inset). Hydrostatic stress in the cell envelope is known to affect molecular processes like stretch-activated channels, however, in extrusion loading, hydrostatic stresses in the cell envelope showed only a small increasing trend with increasing  $\Delta P$ , whereas in gel encapsulation an opposite trend was observed (SI Appendix, Fig. S7). The lack of concurrence between the two loading modalities suggests that hydrostatic stress is not likely the main cause of the mechanically-induced disassembly of CusCBA; this assertion is supported by the fact that CusCBA disassembly during extrusion loading was insensitive to variation in hydrostatic pressure ( $P_{\text{ave}}$ , which primarily regulates cell envelope hydrostatic stress). In contrast, mechanical loading through both extrusion loading and gel encapsulation lead to large increases in cell envelope octahedral shear stress (Fig. 3C-D), suggesting that octahedral shear stress is a likely contributor to disassembly of CusCBA. In materials science, octahedral shear stress is often a useful predictor of material failure. We postulate that octahedral stress within the cell envelope, by promoting distortion of the cell envelope, can facilitate separation of the components of CusCBA and/or modulate the assembly-disassembly kinetics (additional

discussion in SI Appendix, section 1.6). Moreover, the total strain energy imposed on the entire

cell envelope during extrusion loading or in gel encapsulation was on the order of  $10^{-18}$  to  $10^{-13}$ 

kcal, more than sufficient to overcome the energy needed to disrupt all CusCBA complexes in a

cell (about  $10^{-24}$  to  $10^{-23}$  kcal; SI Appendix section 3).

### **Discussion**

322

323

324

325

326327

328

329

330

331

332

333

334

335

336

337

338339

340

341

342

343

344

345

346

347348349

350351

352

353

354

355

356

357

358

359

360

361

362

363364

365

366

367

Using extrusion loading and single-molecule imaging of individual E. coli cells, we have discovered that mechanical stress on the cell disrupts the assembly of CusCBA, a tripartite metal efflux pump that is crucial for resistance to toxic metals, thereby enhancing the effects of copper stress on cell growth. Our finding that octahedral shear stresses (but not hydrostatic stresses) within the cell envelope influence molecular mechanisms further suggests that mechanical loading modalities that primarily generate hydrostatic stress in the cell envelope (e.g., osmotic shock and other variations in turgor pressure; SI Appendix, Fig. S8) may stimulate only a subset of mechano-sensitive mechanisms in bacteria (30). Octahedral shear stresses can develop in the cell envelope following a number of common mechanical events experienced by bacteria in the environment including adhesion to surfaces, overgrowth within crowded cavities, and locomotion. Furthermore, octahedral shear stresses have long been recognized as having distinct effects on physiology; in mammalian systems, octahedral shear stresses have been recognized as having effects on cell, tissue and organ physiology that are distinct form hydrostatic stresses (13, 31). Our findings suggest a broader role for cell envelope stresses in bacteria. Lastly, our findings demonstrate that mechanical stress in the cell envelope can influence trans-envelope protein complexes resulting in physiological changes in bacteria. Trans-envelope protein complexes are ubiquitous in Gram-negative bacteria and their functions ranges from regulating

antibiotic resistance (14, 32, 33), cell division (34), and the translocation of outer membrane components (35). Similar effects of mechanical stresses on these other classes of trans-envelope complexes would suggest that many more physiological mechanisms in bacteria can be sensitive to mechanical forces.

\_

#### **Methods and Materials**

Fabrication and characterization of microfluidic device. A microfluidic device was used to mechanically stimulate individual bacteria (21). Six devices were placed onto each fabricated wafer (SI Appendix, Fig. S1A). The functional units of each device included sixty tapered channels capable of applying extrusion loading at 12 different magnitudes of pressure difference,  $\Delta P$ , and were connected to the device inlet and outlet using feeder channels (SI Appendix, Figs. S1B-D). Tapered channels were designed with an inlet width large enough to permit entry of individual bacteria (1.2  $\mu$ m) and exit widths small enough to inhibit bacterial exit (250 nm). Each tapered channel had a length of 75  $\mu$ m between inlet and outlet. Fluid flow through the bypass channel generated a difference in fluid pressure across each tapered channel.

Sub-micron patterns in the microfluidic devices were fabricated using Deep UV (DUV) lithography at the Cornell Nanoscale Science & Technology Facility. Fused silica was used as a substrate for the microfluidic device to obtain optical clarity and large stiffness. A 55 nm thick chromium etch hard mask was sputter-deposited on silica wafers (500 µm thick, with a 100 mm diameter). A 60 nm thick layer of anti-reflective coating (ARC, DUV 42P) and a 510 nm thick layer of DUV photoresist were deposited on the chromium hard mask using an automated spinner and hot plate system. Exposure of the DUV photoresist was accomplished with a DUV Stepper. The exposed pattern was transferred to the silica substrate using plasma etching. A chrome wet etch was performed to clean off residual chromium. Thru holes were laser-etched into the patterned silica wafer to serve as inlets and outlets.

Depths of device feeder channels were confirmed using a profilometer (*SI Appendix*, Fig. S2A). Tapered channel dimensions were confirmed with SEM and AFM (*SI Appendix*, Figs. S2B-C). The patterned silica wafer was bonded to a thin, bare silica wafer to seal the device (170 µm thickness). Once bonded, wafers were annealed in a furnace. The wafers were allowed to age for a minimum of one week at room temperature before use.

**Strain construction, sample preparation, and device loading.** All strains used in this study were derived from the *E. coli* BW25113 strain (*SI Appendix*, section 1.7). CusA<sup>mE</sup> was created via lambda Red recombineering, where a short, flexible linker L of 10 amino acids (sequence = AGSAAGSGEF) was used to connect mEos3.2-FLAG (a monomeric, irreversibly photoconvertible fluorescent protein mEos3.2 (36, 37) with a C-terminal FLAG tag) to the C-terminus of CusA at its chromosomal locus, as reported in our previous work (18). This CusA<sup>mE</sup> fusion protein is functional and stays intact, as previously shown by cell growth assays and Western blot (18).

To prepare *E. coli* cells expressing mEos3.2-tagged CusA for single-molecule imaging experiments, the cells were first grown in LB medium overnight at 37 °C. The culture was then diluted 1:100 in LB containing chloramphenicol (25  $\mu$ g/mL) and grown at 37 °C for 4 h

(reaching  $OD_{600} = 0.4$ ). The cells were centrifuged down, washed, and re-suspended in 10 mL of M9 medium supplemented with amino acids, vitamins, and glucose (details in *SI Appendix*, section 1.8). The liquid suspension of cells was loaded into the microfluidic device using syringe pumps and capillary tubing under specific pressures (details in *SI Appendix*, section 1.3).

For cell samples requiring copper stress (e.g., in measuring the rate of cell elongation and division), CusA<sup>mE</sup> cell cultures were prepared as described above. The pellet was re-suspended in LB, and CuSO<sub>4</sub> was added to yield a 2.5 mM copper solution. This concentration of copper impacts *E. coli* cell growth but still renders the cells viable.

Imaging experiments and data analysis. Single-molecule tracking (SMT) (38-44) via stroboscopic imaging and single-cell quantification of protein concentration (SCQPC) were performed as previously described (18, 45) on an inverted fluorescence microscope (SI Appendix, Fig. S3 and SI Appendix, section 1.9). For SMT, the cells were first illuminated with a 405 nm laser (1–10 W/cm<sup>2</sup>) for 20 ms to photoconvert a single mEos3.2 molecule (or none) from its green fluorescent form to its red fluorescent form. A series of 30 pulses of a 561 nm laser (21.7 kW/cm<sup>2</sup>) in epi-illumination mode with pulse duration  $t_{int}$  = 4 ms and time lag  $T_{tl}$  = 60 ms were then used to excite the red mEos3.2. The resulting red mEos3.2 fluorescence was imaged by an EMCCD camera, which was synchronized with the 561 nm laser pulses. This imaging scheme was repeated for 500 cycles for each field of view.

After the SMT step, SCQPC was performed on the same cells, in which the cells were illuminated with the 405 nm laser (1–10 W/cm²) for 1 min to photoconvert all remaining mEos3.2 molecules, followed by 561 nm laser illumination for 2000 frames with the same laser power density and exposure time as in the SMT step to quantify the number of remaining mEos3.2 molecules. This 405-illumination and 561-excitation sequence was repeated once more to ensure all mEos3.2 molecules had photobleached. All CusA concentrations cited in the study correspond to those of CusA trimers, i.e., one-third of the total mEos3.2 concentration.

The fluorescence images of individual CusA<sup>mE</sup> molecules from SMT were analyzed within each fitted cell boundary using a home-written MATLAB program, iQPALM (image-based quantitative photo-activated localization microscopy), the details of which have been reported in our previous study (45) and described in *SI Appendix*, sections 1.10 and 1.11). Individual CusA<sup>mE</sup> molecules were identified and position-localized to nanometer precision (typically ~40 nm precision).

**Agarose embedding assay of cell growth.** The procedure for the agarose embedding assay to probe mechanical effects on cell growth was adapted from Auer et al. (28) The appropriate cells were grown at room temperature in gels of a range of agarose concentrations in cuvettes, which give a range of different mechanical rigidity of gel matrix, and in the presence of a range CuSO<sub>4</sub> concentrations (details in *SI Appendix*, section 1.14). The cell growth was monitored by absorbance measurements collected every 30 minutes over a period of 5 hours.

**Statistical information.** Differences among groups were identified using two-tailed ANOVA. Differences between trends were determined using ANCOVA to account for the effects of covariates. Where appropriate, data were submitted to logarithmic transformation to achieve

- 460 normal distributions. Least squares regression models were generated to describe trends.
- Exponential decay rates are determined from nonlinear regression fits to  $y = a_0 + a_1 e^{-x\tau}$ , where  $\tau$
- is the decay rate constant (variance noted using standard error; e.g., Fig. 3A). Unless otherwise
- stated, statistical tests were performed with  $\alpha = 0.05$ . For single-molecule imaging results, the
- data presented included the number of cells measured. Standard deviations are provided in
- relevant figures and tables for data points and fitted parameters.

**Supplementary Information** is available in the online version of this paper.

469 470

468

## Acknowledgements

471 472

473

474

475

476

477

478

479

This study was supported by ARO Grant W911NF-19-1-0121 (P.C. and C.J.H.), NSF Grant CMMI-1463084 (C.J.H.), NIH Grants GM109993 (P.C.), F31AI143208 (L.A.G.), and 5T32GM008500 (L.A.G.). This work was performed in part at the Cornell NanoScale Science and Technology Facility (CNF), a member of the National Nanotechnology Coordinated Infrastructure (NNCI), which is supported by NSF Grant ECCS-1542081. Imaging on the Andor/Olympus Spinning Disk Confocal at the Biotechnology Resource Center (BRC) was supported by NIH Grant 1S10OD010605. We thank the staff at the CNF and BRC for assistance, F. Yang for helping with imaging experiments, K. Gunsallus for finite element modeling assistance, and G. Guisado for measurement assistance.

480 481

### References

482 483

- Thompson DAW & Whyte LL (1942) *On growth and form* (The University Press, Cambridge Eng.).
- 486 2. Heisenberg C-P & Bellaïche Y (2013) Forces in tissue morphogenesis and patterning. *Cell* 153:948-962.
- Vining KH & Mooney DJ (2017) Mechanical forces direct stem cell behaviour in development and regeneration. *Nat Rev Mol Cell Biol* 18:728-742.
- 490 4. Panciera T, Azzolin L, Cordenonsi M, & Piccolo S (2017) Mechanobiology of YAP and TAZ in physiology and disease. *Nat Rev Mol Cell Biol* 18:758-770.
- 492 5. Orr AW, Helmke BP, Blackman BR, & Schwartz MA (2006) Mechanisms of mechanotransduction. *Dev Cell* 10:11-20.
- 494 6. Auer GK & Weibel DB (2017) Bacterial cell mechanics. *Biochemistry* 56:3710-3724.
- 495 7. Sanfilippo JE, *et al.* (2019) Microfluidic-based transcriptomics reveal force-independent bacterial rheosensing. *Nat Microbiol*.
- 497 8. Rodesney CA, *et al.* (2017) Mechanosensing of shear by Pseudomonas aeruginosa leads 498 to increased levels of the cyclic-di-GMP signal initiating biofilm development. *Proc Natl* 499 *Acad Sci USA* 114:5906-5911.
- Rojas ER & Huang KC (2018) Regulation of microbial growth by turgor pressure. *Curr Opin Microbiol* 42:62-70.
- 502 10. Rusconi R, Guasto JS, & Stocker R (2014) Bacterial transport suppressed by fluid shear. 503 *Nat Phys* 10:212-217.

- 504 11. Siryaporn A, Kuchma SL, O'Toole GA, & Gitai Z (2014) Surface attachment induces Pseudomonas aeruginosa virulence. *Proc Natl Acad Sci USA* 111:16860-16865.
- 506 12. Zhou X, *et al.* (2015) Bacterial division. Mechanical crack propagation drives millisecond daughter cell separation in Staphylococcus aureus. *Science* 348:574-578.
- Tambe DT, *et al.* (2011) Collective cell guidance by cooperative intercellular forces. *Nat Mater* 10:469-475.
- 510 14. Zgurskaya HI & Nikaido H (2000) Multidrug resistance mechanisms: drug efflux across two membranes. *Mol Microbiol* 37:219-225.
- 512 15. Mealman TD, Blackburn NJ, & McEvoy MM (2012) Metal export by CusCFBA, the 513 periplasmic Cu(I)/Ag(I) transport system of Escherichia coli. *Curr Top Membr* 69:163-514 196.
- 515 16. Su CC, *et al.* (2011) Crystal structure of the CusBA heavy-metal efflux complex of Escherichia coli. *Nature* 470:558-562.
- 517 17. Outten FW, Huffman DL, Hale JA, & O'Halloran TV (2001) The independent cue and cus systems confer copper tolerance during aerobic and anaerobic growth in Escherichia coli. *J Biol Chem* 276:30670-30677.
- 520 18. Santiago AG, *et al.* (2017) Adaptor protein mediates dynamic pump assembly for bacterial metal efflux. *Proc Natl Acad Sci USA* 114:6694-6699.
- 522 19. Hochmuth RM (2000) Micropipette aspiration of living cells. *J Biomech* 33:15-22.
- 523 20. Needham D & Hochmuth RM (1992) A sensitive measure of surface stress in the resting neutrophil. *Biophys J* 61:1664-1670.
- 525 21. Sun X, Weinlandt WD, Patel H, Wu M, & Hernandez CJ (2014) A microfluidic platform for profiling biomechanical properties of bacteria. *Lab Chip* 14:2491-2498.
- 527 22. Chen TY, *et al.* (2015) Quantifying multistate cytoplasmic molecular diffusion in bacterial cells via inverse transform of confined displacement distribution. *J Phys Chem B* 119:14451-14459.
- Oswald F, E LMB, Bollen YJ, & Peterman EJ (2014) Imaging and quantification of trans-membrane protein diffusion in living bacteria. *Phys Chem Chem Phys* 16:12625-12634.
- 533 24. Mykytczuk NCS, Trevors JT, Leduc LG, & Ferroni GD (2007) Fluorescence polarization 534 in studies of bacterial cytoplasmic membrane fluidity under environmental stress. *Prog* 535 *Biophys Mol Biol* 95:60-82.
- 736 25. Rojas ER, *et al.* (2018) The outer membrane is an essential load-bearing element in Gram-negative bacteria. *Nature* 559:617-621.
- Trivedi RR, *et al.* (2018) Mechanical genomic studies reveal the role of D-alanine metabolism in Pseudomonas aeruginosa cell stiffness. *MBio* 9:e01340-01318.
- 540 27. Wong F, *et al.* (2017) Mechanical strain sensing implicated in cell shape recovery in Escherichia coli. *Nat Microbiol* 2:17115.
- 542 28. Auer GK, *et al.* (2016) Mechanical genomics identifies diverse modulators of bacterial cell stiffness. *Cell Syst* 2:402-411.
- Tuson HH, *et al.* (2012) Measuring the stiffness of bacterial cells from growth rates in hydrogels of tunable elasticity. *Mol Microbiol* 84:874-891.
- 546 30. Cox CD, Bavi N, & Martinac B (2018) Bacterial mechanosensors. *Annu Rev Physiol* 80:71-93.
- 548 31. Pauwels F (1980) *Biomechanics of the locomotor apparatus : contributions on the functional anatomy of the locomotor apparatus* (Springer-Verlag, Berlin; New York).

- Solution 32. Routh MD, et al. (2011) Efflux pumps of the resistance-nodulation-division family: a perspective of their structure, function, and regulation in gram-negative bacteria. Adv Enzymol Relat Areas Mol Biol 77:109-146.
- 553 33. Piddock LJ (2006) Multidrug-resistance efflux pumps not just for resistance. *Nat Rev Microbiol* 4:629-636.
- Gerding MA, Ogata Y, Pecora ND, Niki H, & de Boer PA (2007) The trans-envelope
   Tol-Pal complex is part of the cell division machinery and required for proper outer membrane invagination during cell constriction in E. coli. *Mol Microbiol* 63:1008-1025.
- 558 35. Freinkman E, Okuda S, Ruiz N, & Kahne D (2012) Regulated assembly of the transenvelope protein complex required for lipopolysaccharide export. *Biochemistry* 51:4800-4806.
- 561 36. Zhang M, *et al.* (2012) Rational design of true monomeric and bright photoactivatable fluorescent proteins. *Nat Methods* 9:727-729.
- 563 37. McKinney SA, Murphy CS, Hazelwood KL, Davidson MW, & Looger LL (2009) A bright and photostable photoconvertible fluorescent protein. *Nat Methods* 6:131-133.
- 565 38. Elf J, Li GW, & Xie XS (2007) Probing transcription factor dynamics at the single-566 molecule level in a living cell. *Science* 316:1191-1194.
- 567 39. English BP, *et al.* (2011) Single-molecule investigations of the stringent response machinery in living bacterial cells. *Proc Natl Acad Sci USA* 108:E365-373.
- Mehta P, *et al.* (2013) Dynamics and stoichiometry of a regulated enhancer-binding protein in live Escherichia coli cells. *Nat Commun* 4:1997.
- 571 41. Bakshi S, Bratton BP, & Weisshaar JC (2011) Subdiffraction-limit study of Kaede diffusion and spatial distribution in live Escherichia coli. *Biophys J* 101:2535-2544.
- Mazza D, Abernathy A, Golob N, Morisaki T, & McNally JG (2012) A benchmark for chromatin binding measurements in live cells. *Nucleic Acids Res* 40:e119.
- Javer A, *et al.* (2013) Short-time movement of E. coli chromosomal loci depends on coordinate and subcellular localization. *Nat Commun* 4:3003.
- 577 44. Gahlmann A & Moerner WE (2014) Exploring bacterial cell biology with single-578 molecule tracking and super-resolution imaging. *Nat Rev Microbiol* 12:9-22.

579 45. Chen TY, *et al.* (2015) Concentration- and chromosome-organization-dependent 580 regulator unbinding from DNA for transcription regulation in living cells. *Nat Commun* 581 6:7445.